

Elucidating the Photophysics and Nonlinear Optical Properties of a Novel Azo Prototype for Possible Photonic Applications: A Quantum Chemical Analysis

Sávio Fonseca, Neidy S. S. dos Santos, Herbert C. Georg, Tertius L. Fonseca, Patricio F. Provasi, Kaline Coutinho, Sylvio Canuto, Antônio R. da Cunha, and Rodrigo Gester*

Cite This: <https://doi.org/10.1021/acsomega.4c04240>

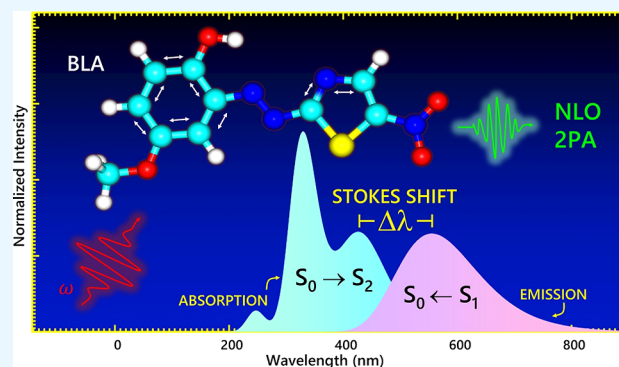
Read Online

ACCESS |

Metrics & More

Article Recommendations

ABSTRACT: The photophysics and nonlinear optical responses of a novel nitrothiazol-methoxyphenol molecule were investigated using density functional theory (DFT) and time-dependent density functional theory (TD-DFT) methods with the polarizable continuum model to take the solvent effect into account. Special attention is paid to the description of the lowest absorption band, characterized as a strong $\pi \rightarrow \pi^*$ state in the visible region of the spectrum. The TD-DFT emission spectrum analysis reveals a significant Stokes shift of more than 120 nm for the $\pi \rightarrow \pi^*$ state in gas phase condition. The results show a great influence of the solvent polarity on the nonlinear optical (NLO) response of the molecule. Specifically, the second harmonic generation hyperpolarizability $\beta(-2\omega; \omega, \omega)$ shows a large variation from gas to aqueous solvent (82×10^{-30} to 162×10^{-30} esu), exhibiting notably higher values than those reported for standard compounds such as urea (0.34×10^{-30} esu) and *p*-nitroaniline (6.42×10^{-30} esu). Furthermore, a two-photon absorption analysis indicates a large cross-section ($\delta^{2PA} = 77$ GM) with superior performance compared to several dyes. These results make the molecule quite interesting for nonlinear optics.



1. INTRODUCTION

Nonlinear optical (NLO) molecules and materials have been a continuous source of research for the past three decades, driven by their potential applications in optoelectronics, photonics, and communication technologies, such as optical data processing and storage.^{1–4} They are also attracting growing interest for possible applications in bioimaging, since the second harmonic generation (SHG) technique can produce high-resolution images from deep within biological tissues.^{5–7} Among the various NLO chromophores, SHG probes are typically designed by incorporating donor (D) and acceptor (A) groups, linked via a π -system, which provides the asymmetry required for quadratic NLO phenomena. These materials are not only synthetically accessible but they also have low dielectric constant and fast electronic responses, making them preferable to inorganic materials. Understanding, controlling and optimizing the NLO responses of organic compounds is fundamental, requiring experimental and quantum chemical characterizations to elucidate NLO structure–property relationships, including the influence of donor and acceptor forces and the nature of the π -conjugated segment.^{8–17}

On the other hand, given that experimental property determination typically occurs in condensed phases, it is crucial to examine how environmental factors, such as the effects of solvents, impact NLO responses. Experimental studies have demonstrated that solvent effects can significantly alter the NLO response, as evidenced by compounds like *para*-nitroaniline (PNA), donor–acceptor polyenes, and thiophene chromophores.^{18–23} From these studies, it has been observed that more polar solvents tend to enhance the NLO responses. This highlights the need to take into account the effects of solvents in the design and application of NLO materials. Solvatochromism is an example of how a solvent can influence a specific molecular property. Solvatochromic effects arise from interactions between solute and solvent, leading to changes in the shape, intensity, and position of spectral lines.²³ In this

Received: May 3, 2024

Revised: September 2, 2024

Accepted: September 13, 2024

study, we utilized implicit schemes where the solvent is modeled as a polarizable continuum medium, characterized by its macroscopic properties, such as the dielectric constant.²⁴

Quantum chemical studies on the physicochemical properties of NLO molecules provide complementary information to understand the relationships between their structural, electronic, and optical properties and therefore to design new molecules.¹ In this context, 2-[2'-(5-nitrothiazolyl)azo]-4-methoxyphenol (NTAMP) depicted in Figure 1 emerges as a

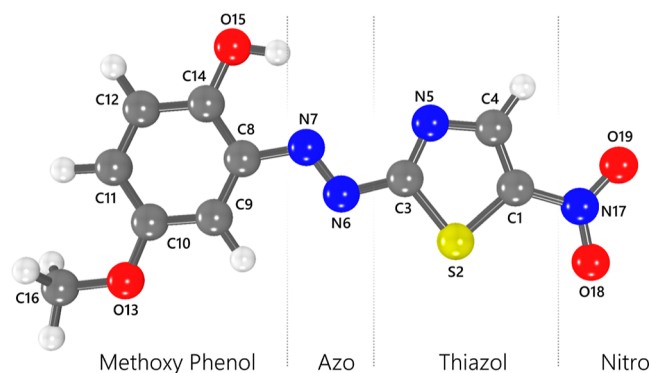


Figure 1. Molecular structure of the NTAMP molecule.

challenge.²⁵ Despite being a potential prototype for novel devices, none of its optical properties have been investigated yet. Furthermore, even when the knowledge of the electronic structure of NTAMP has advanced, there is no information on how the environment influences these properties. It has been observed that this compound presents strong and broad excitation in the visible spectral region. However, contrary to expectations, this transition has been assigned as a weak state $n \rightarrow \pi^*$, which is puzzling, since these excitation types are not usually associated with strong intensities.

To better understand certain aspects of NTAMP photo-physics, we drive a detailed investigation of its optical properties using theoretical quantum chemical methods. We particularly focus on the solvent and how its interactions can modulate the optical parameters of interest. Furthermore, we consider both the static field and the frequency-dependent light, which are crucial to understanding the effects of the SHG.²⁶ Although they contradict the original assignment, all the used density functional theory (DFT) approaches have identified the three low-lying electronic bands observed previously experimentally and, instead, we find that it is a strong excitation $\pi \rightarrow \pi^*$. Additionally, despite the substantial values of the Stokes shift coefficients and NLO estimated for this azo compound, the solvent enhances these parameters, suggesting potential applications such as sensors, molecular probes, and optical devices such as sensors, and organic light-emitting diodes, or even solar cells.

2. METHODOLOGY

The NLO parameters of interest are the first hyperpolarizability (β) and the two-photon cross-section (δ). The first of them is a three rank tensor with 27 components. At static conditions or frequency-independent light, a representative quantity related to this tensor is given as²⁶

$$\beta_{\text{total}} = \sqrt{\beta_x^2 + \beta_y^2 + \beta_z^2} \quad (1)$$

where

$$\beta_i = \beta_{iii} + \frac{1}{3} \sum (\beta_{ijj} + \beta_{jij} + \beta_{jji}) \quad (2)$$

Another very important quantity for photonics, related to the second-harmonic generation phenomenon, is the frequency-dependent first hyperpolarizability, $\beta(-2\omega; \omega, \omega)$.²⁶ For frequency-dependent light, this optical coefficient can be obtained within the hyper-Rayleigh scattering (HRS) formalism as²⁷

$$\beta_{\text{HRS}} = \sqrt{\frac{10}{45} |\beta_{j=1}|^2 + \frac{10}{105} |\beta_{j=3}|^2} \quad (3)$$

In this equation, $\beta_{j=1}$ and $\beta_{j=3}$ parameters correspond respectively to the dipolar and octupolar tensors, respectively written like

$$|\beta_{j=1}|^2 = \frac{3}{5} \sum_i^{x,y,z} \beta_{iii}^2 + \frac{6}{5} \sum_{i \neq j}^{x,y,z} \beta_{iii} \beta_{jjj} + \frac{3}{5} \sum_{i \neq j}^{x,y,z} \beta_{jii}^2 + \frac{3}{5} \sum_{i \neq j \neq k}^{x,y,z} \beta_{ijj} \beta_{ikk} \quad (4)$$

and

$$|\beta_{j=3}|^2 = \frac{2}{5} \sum_i^{x,y,z} \beta_{iii}^2 - \frac{6}{5} \sum_{i \neq j}^{x,y,z} \beta_{iii} \beta_{jjj} + \frac{12}{5} \sum_{i \neq j}^{x,y,z} \beta_{jii}^2 - \frac{3}{5} \sum_{i \neq j \neq k}^{x,y,z} \beta_{ijj} \beta_{ikk} + \sum_{i \neq j \neq k}^{x,y,z} \beta_{jij}^2 \quad (5)$$

These two tensors can be combined to give the anisotropic factor $\rho = |\beta_{j=3}|/|\beta_{j=1}|$, defining the dipolar, $\Phi_{j=1} = 1/(1 + \rho)$, and octupolar, $\Phi_{j=3} = \rho/(1 + \rho)$ contributions to the first hyperpolarizability.

Calculations of the first hyperpolarizability were performed in Gaussian 16 code²⁸ considering different DFT-based methods and the 6-311++G(d,p) basis set. Finally, the optical coefficients were posteriorly analyzed using the Multiwfn program.²⁹ The same setup was applied to obtain the electronic excitations.

The effect of the solvent on the two-photon absorption mechanism (2PA) was also accounted for. It is a third-order phenomenon related to applications like photodynamic therapy, communication devices, telecommunications, integrated chips, and so on.³⁰

Within the quantum mechanics formalism, 2PA is studied using a time-dependent perturbation theory. Considering a monochromatic linearly polarized light, the two-photon cross-section ($\delta_{\text{a.u.}}^{2\text{PA}}$) is given as a transition from $|0\rangle$ to $|f\rangle$ as

$$\delta_{\text{a.u.}}^{2\text{PA}} = 2 \sum_{\alpha, \beta} (S_{\alpha\alpha}^{\text{of}} S_{\beta\beta}^{\text{of}} + 2S_{\alpha\beta}^{\text{of}} S_{\alpha\beta}^{\text{of}}) \quad (6)$$

In this equation, the indices α and β over the three Cartesian coordinates, being $S_{\alpha\beta}^{\text{of}}$ the $\alpha\beta$ -th component of the two-photon tensor, which the mathematical form is given as

$$S_{\alpha\beta}^{\text{of}} = \sum_n \frac{\mu_{\alpha}^{\text{of}} \mu_{\beta}^{\text{nf}} + \mu_{\beta}^{\text{of}} \mu_{\alpha}^{\text{nf}}}{\omega_{0n} - \omega_{\text{of}}/2} \quad (7)$$

where μ_a^{pq} and ω_{pq} are, respectively, the a -th component of the one-photon transition moment and the excitation energy for a transition going from $|p\rangle$ to $|q\rangle$. Note that $\delta_{\text{a.u.}}^{2\text{PA}}$ is in

atomic units, but it can be transformed to GM (Göppert-Mayer) units by the following relation

$$\delta_{\text{GM}}^{2\text{PA}} = \frac{N\pi^3\alpha_0^5\omega^2}{c}g(2\omega, \omega_0, \Gamma)\delta_{\text{a.u.}}^{2\text{PA}} \quad (8)$$

In this context, N is an integer that depends on the experimental setup, a is the fine structure constant, a_0 is the Bohr radius, ω is the energy of the incoming photon, c is the speed of light, and $g(2\omega, \omega_0, \Gamma)$ is the line-shape function. All calculations for 2PA were carried out using the Dalton program³¹ and the 6-311++G(d,p) basis set.

All molecular geometries were obtained within the DFT framework^{32–34} using the ω B97XD method^{35,36} with the Pople 6-311++G(d,p) basis set.^{37,38} We have computed the geometry of the first excited state to investigate the emission excitation. In addition, the electronic properties considered here were also calculated using the M06-2X,³⁹ and CAM-B3LYP⁴⁰ methods. The solvent effects on the geometry and electronic properties were taken into account using the integral-equation version of the polarizable continuum model (PCM).^{24,41,42}

The calculation of hyperpolarizability has consistently presented challenges, especially for compounds with donor and acceptor substituents due to the inherently nonlocal nature of their response. The CAM-B3LYP,⁴⁰ M06-2X³⁹ and ω B97XD^{35,36} functionals belong to a new class of DFT functionals known as range-separated functionals, which effectively capture both short-range and long-range interactions.^{43,44}

3. RESULTS AND DISCUSSION

3.1. Geometry Analysis. The environment can affect diverse molecular properties, both directly, without appreciable modifications in the geometry of the solute, and indirectly, by inducing significant changes in the solute geometry. In particular, molecules with electron donor and acceptor moieties connected by a π -electron bridge may be largely affected by polar environments.^{45,46} In some cases, drastic geometric changes may occur upon solvation, leading the solute molecules to a cyanine-like state⁴⁷ or even to a zwitterionic state.^{45,46} NLO properties may also suffer drastic changes as a result of both the direct and indirect solvent effects.⁴⁷

Table 1 shows all the bond lengths of NTAMP and two bond length alternation (BLA) coordinates, selected to monitor the structure of the phenol and thiazol rings, respectively. The BLA coordinates, χ_{P} and χ_{T} , are defined as

$$\chi_{\text{P}} = \frac{1}{4}[r(\text{C}_9 - \text{C}_{10}) + r(\text{C}_{10} - \text{C}_{11}) + r(\text{C}_{12} - \text{C}_{14}) + r(\text{C}_8 - \text{C}_{14}) - 2 \cdot r(\text{C}_8 - \text{C}_9) - 2 \cdot r(\text{C}_{11} - \text{C}_{12})] \quad (9)$$

$$\chi_{\text{T}} = r(\text{C}_4 - \text{N}_5) - r(\text{C}_3 - \text{N}_5) \quad (10)$$

The χ_{P} BLA coordinate gives us information about the general state of the phenyl ring. As discussed in a previous paper,⁴⁷ when χ_{P} is near zero, the ring is aromatic, while a value near 0.1 Å means that the ring is quinoidal, with the symmetry axis of the quinoidal ring being along the bonds $\text{C}_{14}-\text{O}_{15}$ and $\text{C}_{10}-\text{O}_{13}$. The χ_{T} BLA coordinate, in its turn, gives us information about the conjugation state of the N–C bonds in thiazol ring. A positive value of χ_{T} , around 0.07 Å, means that C_4-N_5 is a single bond and C_3-N_5 is a double bond, as expected for the molecule in normal, nonzwitterionic

Table 1. Bond Length and Bond Length Alternation (BLA) Coordinates, in Å, Obtained for NTAMP in Gas Phase and Solvent for the Ground and First Excited States Calculated with TD- ω B97XD/6-311++G(d,p)

	ground state		emission state	
	gas phase	water	gas phase	water
Bond Lengths				
C_1-S_2	1.720	1.720	1.737	1.727
C_1-C_4	1.365	1.367	1.365	1.384
C_4-N_5	1.355	1.353	1.356	1.327
C_3-N_5	1.305	1.308	1.329	1.342
S_2-C_3	1.732	1.728	1.748	1.761
C_3-N_6	1.401	1.400	1.332	1.330
N_6-N_7	1.249	1.249	1.233	1.305
N_7-C_8	1.391	1.391	1.366	1.367
C_8-C_9	1.399	1.400	1.399	1.376
C_9-C_{10}	1.381	1.382	1.385	1.409
$\text{C}_{10}-\text{C}_{11}$	1.405	1.406	1.397	1.418
$\text{C}_{10}-\text{O}_{13}$	1.358	1.357	1.358	1.325
$\text{C}_{11}-\text{C}_{12}$	1.385	1.384	1.389	1.376
$\text{C}_{12}-\text{C}_{14}$	1.391	1.391	1.381	1.398
C_8-C_{14}	1.408	1.408	1.408	1.441
$\text{C}_{14}-\text{O}_{15}$	1.341	1.345	1.353	1.315
C_1-N_{17}	1.438	1.430	1.420	1.397
$\text{N}_{17}-\text{O}_{18}$	1.218	1.221	1.220	1.233
$\text{N}_{17}-\text{O}_{19}$	1.215	1.218	1.224	1.235
BLAs				
χ_{P}	0.005	0.005	−0.001	0.040
χ_{T}	0.050	0.045	0.027	−0.015

state. A pronounced negative value of χ_{T} means that the N–C bonds in the thiazol ring are reversed, which means that the molecule is in a zwitterionic state.

Now, from Table 1 we observe that no significant change occurs in any bond length, in the ground state, upon solvation. Both in gas phase and in water, χ_{P} is very close to zero, which means an aromatic phenyl ring and χ_{T} is around 0.05 Å, which means a pronounced single–double conjugation in the N–C bonds in the thiazol ring. Also, the N_6-N_7 bond length is around 1.25 Å, which is very typical of a double bond. Therefore, these results indicate that NTAMP suffers no appreciable charge separation in the ground state upon solvation.

On the other hand, for the emission state, that is, the minimum energy geometry of the first excited state, the picture is quite different. Many bond lengths change appreciably upon solvation. In particular, χ_{P} , which is essentially zero in gas phase, increases to 0.04 Å in water, showing that the phenyl ring changes to a structure that lies in the midway between aromatic and quinoidal. Accordingly, the bonds $\text{C}_{10}-\text{O}_{13}$ and $\text{C}_{14}-\text{O}_{15}$ also suffer a significant decrease, assuming a more double-bond character, which is in line with the more quinoidal structure of the phenyl ring. The other BLA coordinate, χ_{T} , changes from 0.027 Å in gas phase to −0.015 Å in water, which means that the single–double conjugation in the N–C bonds in the thiazol ring are inverted. Also, the N_6-N_7 bond suffers a large increase from 1.233 to 1.305 Å, which is a significant change toward a single bond character.

These results show that, in the emission state, NTAMP undergoes a significant charge separation upon solvation. However, for characterizing a zwitterionic state, we would expect χ_{P} to be closer to 0.1 Å and χ_{T} closer to −0.07 Å. Also,

Table 2. Lowest Absorption and Emission Bands, as Well as the Stokes Shifts Calculated for the NTAMP Molecule at Gas Phase and Aqueous Conditions

method		absorption ($\pi \rightarrow \pi^*$)			emission ($\pi \leftarrow \pi^*$)			Stokes Shift
		λ_{abs} (nm)	Osc.	contribution	λ_{em} (nm)	Osc.	contribution	$\Delta\lambda = \lambda_{\text{em}} - \lambda_{\text{abs}}$ (nm)
M06-2X	gas	($S_0 \rightarrow S_2$)428.9	0.319	H \rightarrow L (93%)	($S_0 \leftarrow S_1$)555.2	0.247	H \leftarrow L (96%)	126.3
	water	($S_0 \rightarrow S_2$) 462.0	0.621	H \rightarrow L (90%)	($S_0 \leftarrow S_1$) 651.3	0.699	H \leftarrow L (96%)	189.3
CAM-B3LYP	gas	($S_0 \rightarrow S_2$) 443.1	0.302	H \rightarrow L (91%)	($S_0 \leftarrow S_1$) 576.4	0.239	H \leftarrow L (95%)	124.3
	water	($S_0 \rightarrow S_2$) 479.1	0.594	H \rightarrow L (87%)	($S_0 \leftarrow S_1$) 677.4	0.680	H \leftarrow L (95%)	234.3
ω B97XD	gas	($S_0 \rightarrow S_2$) 434.3	0.321	H \rightarrow L (88%)	($S_0 \leftarrow S_1$) 560.1	0.256	H \leftarrow L (93%)	125.8
	water	($S_0 \rightarrow S_2$) 469.6	0.620	H \rightarrow L (84%)	($S_0 \leftarrow S_1$) 662.5	0.706	H \leftarrow L (93%)	192.9

the N₆–N₇ bond should be closer to 1.4 Å, that is a typical value for a single N–N bond. Therefore, we conclude that the molecule does not reach a zwitterionic state, but rather a cyanine-like state, which is in between the normal, non charge separated state and the zwitterionic state.

3.2. Electronic Transitions and Stokes Shift. Waheeb and collaborators have reported the electronic absorption spectra of the NTAMP molecule²⁵ and identified a broad and intense band at 397 nm. The authors assigned this excitation as a $n \rightarrow \pi^*$, which is questionable, as this type of transition generally exhibits low intensity.

To elucidate the electronic transitions and have a better understanding of NTAMP's photophysics, we have performed time-dependent density functional theory calculations with the molecule both in gas phase and in water. A summary of the results is presented in Table 2. The results for the absorption with the M06-2X functional show the presence of a $S_0 \rightarrow S_1$ transition lying at 494.5 nm with an $n \rightarrow \pi^*$ symmetry. This is confirmed by the results obtained with CAM-B3LYP and ω B97XD which also indicate that this transition has null oscillator strength, thus being a black state that does not appear in the absorption spectra. Consequently, this excitation is not meaningful, and therefore, omitted in Table 2.

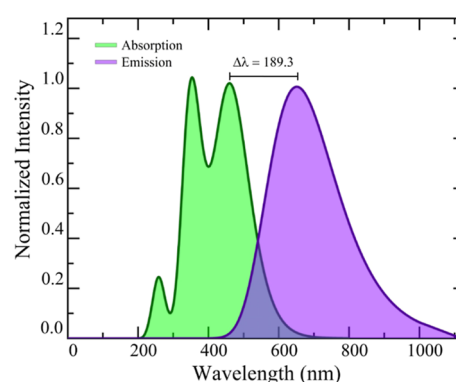
Additionally, Figure 2 illustrates the electronic absorption and emission spectra calculated in gas phase and aqueous solution. The band observed at 428.9 nm for the isolated molecule exhibits a strong oscillator strength of 0.319. However, after analyzing the molecular orbitals as depicted in Figure 3, it becomes clear that this excitation is not a $n \rightarrow \pi^*$ transition as previously assigned, but rather a $\pi \rightarrow \pi^*$ transition.

We obtained the minimum energy geometry in the lowest excited state and it corresponds to the same $\pi \rightarrow \pi^*$ state. The emission then is calculated at 555.2 nm, suggesting a large Stokes shift, with $\Delta\lambda = \lambda_{\text{em}} - \lambda_{\text{abs}} = 126.3$ nm.

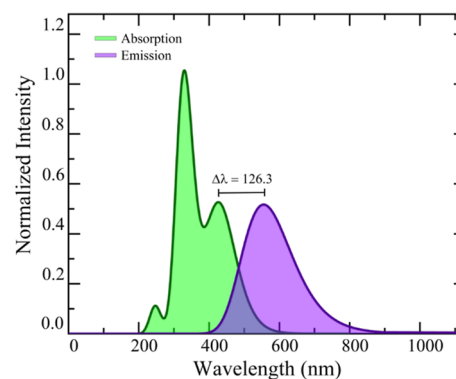
The solvent environment has a significant impact on the electronic excitations of NTAMP. The most noticeable effect comes from the intensities of the transitions. According to the experimental results obtained in methanol, the lowest absorption band should be the most intense, which is not observed in the gas phase spectrum shown in Figure 2a. However, including polarization effects using PCM helps to address this issue, as illustrated in Figure 2b.

In addition, the solvent moves this absorption band to 462 nm, a bathochromic shift of 33.1 nm compared to the gas phase molecule. The fluorescence also occurs at lower energies, specifically at 651.3 nm, resulting in a Stokes shift of 189.3 nm, indicating an improvement compared to the same Stokes shift in the gas phase condition.

3.3. Intramolecular Charge-Transfer. A pronounced intramolecular charge transfer (ICT) is likely to occur in



(a) Gas phase



(b) Aqueous solution

Figure 2. Electronic emission and absorption spectra calculated at the M06-2X/6-311++G(d,p) level for NTAMP in gas phase and aqueous solution.

molecules possessing a D- π -A structure, upon interaction with polar environments or following transitions to some excited states. And such charge transfer is quite relevant for understanding molecular solvatochromism and the effects in NLO properties.

As shown in Table 3, the ground state dipole moment in the gas phase is 6.5 D. However, following a vertical excitation, the dipole moment increases to 14.9 D, indicating a large polarization of the electronic charge.

Figure 4 shows the electron density difference ($\Delta\rho$) between the FC excited state and the ground state of the isolated molecule. We observe that there is a significant migration of electron density from the methoxy phenol moiety of the molecule to the other moiety, clearly characterizing the $\pi \rightarrow \pi^*$ excited state as an ICT state.

In water, these effects are more pronounced. For example, the ground state dipole moment is now computed as 8.0 D, indicating a polarization, attributed to the solvent, of

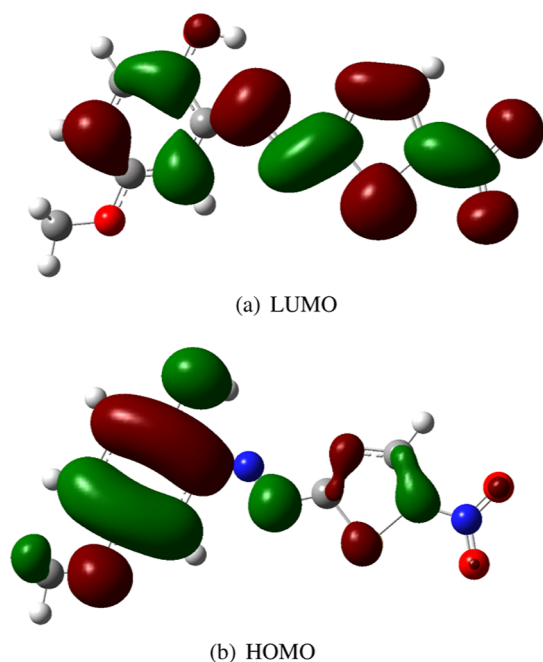


Figure 3. Kohn–Sham molecular orbitals involved in the lowest absorption and emission bands.

Table 3. Ground State (GS) and Franck–Condon State (FC) Dipole Moments (μ/D)

method	gas phase		water	
	μ_{GS}	μ_{FC}	μ_{GS}	μ_{FC}
M06-2X	6.5	14.9	8.0	19.3
CAM-B3LYP	6.6	14.8	8.1	19.2
ω B97XD	6.5	14.1	8.0	18.2

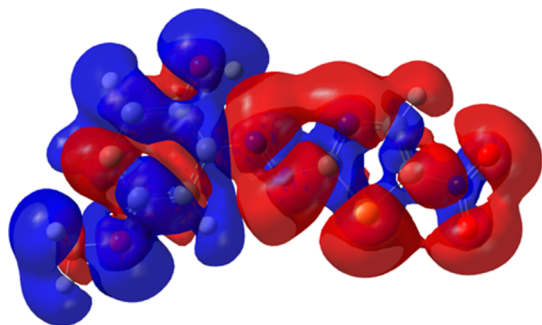


Figure 4. Electron density difference ($\Delta\rho$) between the FC excited state and the ground state computed with TD-CAM-B3LYP/6-311++G(d,p) in gas phase. In red it shows the regions of density increase, while in blue the regions of density decrease. A visualization threshold of 0.0001 au was applied.

approximately 20%. In contrast, the Franck–Condon excited state exhibits a value of 19.3 D, approximately 39% greater than the gas phase value. Thus, the solvent further enhances the ICT phenomenon.

3.4. First Hyperpolarizability. Table 4 presents the results for the static (β_{total}) and frequency-dependent (β_{HRS}) first hyperpolarizabilities, enabling analysis of the chromophore's performance. Static hyperpolarizabilities represent an inherent material response, independent of the incident radiation. Under gas phase conditions, a large value of 45×10^{-30} esu is obtained. For comparison, our DFT results for the

first static hyperpolarizability are comparable to the second-order Møller–Plesset perturbation theory (MP2) results for azo-enaminone compounds of around 50×10^{-30} esu,¹⁰ where the azo group plays an important role in the nonlinear activities of the system. However, considering the presence of the solvent, this parameter is considerably increased to 133×10^{-30} esu, signifying a large polarization effect of 196% relative to the isolated molecule. This finding is consistent with previous studies showing that solvent effects can significantly increase the NLO response, as demonstrated for azochromophore with tricyanopyrrole acceptor moiety,⁴⁸ twisted Möbius annulenes,⁴⁹ organic biphotochrome,⁵⁰ push–pull phenylpolyenes,⁵¹ pyridinium-*N*-phenoxide betaines⁵² and organic molecules.⁵³ Additionally, it is noteworthy that NTAMP performs exceptionally well compared to other standard optical materials. For example, the first hyperpolarizabilities of urea and *p*-nitroaniline have been reported as 0.3×10^{-30} and 6.4×10^{-30} esu, respectively.^{54,55} Therefore, NTAMP appears to be a promising compound for NLO applications.

The impact of incident radiation can be assessed by analyzing the HRS data. The results presented in Table 4 were calculated for a laser of frequency $\lambda = 1064$ nm, which is most commonly used in experimental measurements. Under gas phase conditions, β_{HRS} yields 68×10^{-30} esu. However, when the NTAMP molecule is in aqueous solution, this value changes to 128×10^{-30} esu, again indicating a large polarization effect of 88%. This is lower than that obtained for the static case, but still a substantial effect of the solvent on the molecular NLO performance.

We can obtain a qualitative interpretation of the solvent effect on the first hyperpolarizability by considering the two-level model¹

$$\beta^{\text{TL}} = \frac{3 f_0 \Delta\mu}{2 \Delta E^3} \quad (11)$$

where ΔE , f_0 and $\Delta\mu$ are, respectively, the transition energy, the oscillator strength, and the difference between the permanent dipole moments of the excited state and the ground state. This model establishes a link between the first hyperpolarizability and the so-called crucial electronic transitions. Here, the crucial electronic transition is characterized by small excitation energy, large f_0 and large $\Delta\mu$. Tables 2 and 3 also report the DFT spectroscopic factors of the two-level model calculated in gas phase and aqueous solution. At the M06-2X level, for instance, the values of β^{TL} for NTAMP are in the increasing order of gas phase (11.4×10^{-30} esu) < water (37.3×10^{-30} esu), which is in agreement with the order of values of the dominant component, β_{xxx} : gas phase (43.1×10^{-30} esu) < water (132.1×10^{-30} esu). Also, we observe that the values of β^{TL} is due to the combination of the oscillator strength and the charge transfer of the crucial transition.

Finally, a relevant aspect pertains to the origins of the first hyperpolarizability. This aspect can be better understood by leveraging the depolarization ratio (DR), which ranges from 1.5 (octupolar) to 9 (dipolar), delineating the nature of these contributions. As per Table 4, all addressed quantum mechanical methods indicate values around DR = 5, regardless of the environment. Furthermore, based on the dipolar ($\Phi_{J=1}$) and octupolar contributions ($\Phi_{J=3}$), there exists a balance between these compositions. However, Zhang and collaborators²⁷ devised a scale that more accurately classifies NTAMP as a dipolar compound.

Table 4. First Hyperpolarizability ($\beta/10^{-30}$ esu), Energy Gap (eV), Depolarization Ration (DR), Anisotropy Ratio (ρ), Dipolar ($\Phi_{J=1}$), and Octupolar ($\Phi_{J=3}$) contributions^{ab}

property	M06-2X		CAM-B3LYP		ω B97XD	
	gas	water	gas	water	gas	water
β_{total}	44.61	133.28	47.15	145.77	43.04	131.09
β_x	-43.74	-130.26	46.23	-142.50	-42.13	-127.88
β_y	87.78	28.27	9.24	30.71	8.78	28.84
β_z	0.00	0.00	0.00	0.00	0.00	0.00
β_{HRS}	68.00	127.51	81.85	162.93	68.01	129.62
DR	5.00	5.02	5.01	5.03	5.02	5.04
E_{gap}	4.65	4.61	4.93	4.87	6.08	6.01
$\Phi_{J=1}$	0.551	0.552	0.551	0.552	0.552	0.553
$\Phi_{J=3}$	0.449	0.448	0.449	0.448	0.448	0.447
ρ	0.81	0.81	0.81	0.81	0.81	0.81

^aThe frequency-dependent results were calculated at $\lambda = 1064$ nm. ^bThe converting value for β are 1 au = 8.63922×10^{-33} esu.

Table 5. Two-Photon Absorption Cross-Section Calculated at the CAM-B3LYP/6-311++G(d,p) Level of Theory^a

environment	transition	energy (eV)	two-photon tensor elements						$\delta_{\text{a.u.}}^{2\text{PA}}$	$\delta_{\text{GM}}^{2\text{PA}}$
			S_{xx}	S_{yy}	S_{zz}	S_{xy}	S_{xz}	S_{yz}		
gas phase	1	2.68	0.0	0.0	-0.0	-0.0	3.3	-0.4	0.02	0.03
	2	2.80	-180.8	-3.5	0.2	41.4	0.0	-0.0	40.7	77.20
water	1	2.56	-435.2	-17.0	0.7	106.6	0.0	-0.0	202	383.15
	2	2.65	-0.0	-0.0	-0.0	0.0	7.4	-0.9	0.08	0.15

^aThe factors of conversion are 1 au = 1.896788×10^{-50} cm⁴ s/photon, and 1 GM = 10^{-50} cm⁴ s/photon.

3.5. Two-Photon Absorption Cross-Section. Table 5 shows the results for the fourth lowest two-photon absorption transitions calculated for the NTAMP molecule in both gas phase and water solvent. The first transition exhibits a negligible cross-section of 0.03 GM at 2.68 eV (462.6 nm), corresponding to the $n \rightarrow \pi^*$ excitation as predicted by theoretical calculations but not observed in the experiment.

The highest 2PA value (77.2 GM) is observed at 2.80 eV (442.8 nm), which coincides with the energy of the lowest $\pi \rightarrow \pi^*$ transition responsible for the broad absorption band in the visible spectrum. The contributions of S_{xx} and S_{xy} to this effect are significant, with values of -180.8 and 41.4 au, respectively. However, considering a recent study that compared the performances of CAM-B3LYP, CC2, and EOM-EE-CCSD methods with different basis sets,⁵⁶ a higher value is expected. According to these findings, the outcomes obtained with CAM-B3LYP are potentially three times lower than those obtained with more advanced techniques like CC2 and EOM-EE-CCSD. Moreover, it is feasible to expect cross-section values of 231.6 GM.

In the aqueous environment, the 2PA cross-section increases considerably. The CAM-B3LYP results associated with the PCM indicate a value of 385.15 GM at 2.56 eV (484.31 nm). That means a strong redshift regarding the gas-phase spectra.

In comparison to other dyes, NTAMP demonstrates enhanced performance. For instance, when considering the pNA molecule, experimental and theoretical methodologies suggest values ranging from 8.04 to 12.17 GM depending on the solvent environment.⁵⁷ First-principle Born–Oppenheimer Molecular Dynamics indicate that these values may be even lower in a water solvent, between 4.4 and 10.3 GM.⁵⁸ In contrast, the predicted values for NTAMP are notably higher than other dyes functionalized to exhibit increased 2PA. This is evident in the case of certain nanosubstituted chalcones,⁵⁹ dibenzylideneacetone, and thiosemicarbazone derivatives.^{54,60}

4. CONCLUSIONS

We carried out a systematic quantum chemical investigation on the effects of solvents on the linear and nonlinear optical properties of NTAMP, a recently synthesized azo compound. Photophysical analysis reveals three notable findings.

The nature of the lowest absorption band, previously assigned as a weak $n \rightarrow \pi^*$ transition, was investigated. Unlike previous predictions, quantum chemical calculations based on DFT theory show that this band is, in fact, a $\pi \rightarrow \pi^*$ state.

The emission spectra of NTAMP were also discussed, highlighting some significant aspects of its photophysics. For example, even in the gas phase, all results indicated a Stokes shift of approximately 125 nm. Furthermore, solute–solvent interactions act to enhance this property. While there are no experimental discussions on the efficiency of this molecule in capturing the emission of light electric current, the reported large Stokes shift and the higher intensity of the lower excitation band suggest potential applications such as sensors, biological probes, light emitting diodes, or solar cells.

Special attention was paid to the first hyperpolarizability, often considered the most relevant nonlinear optical parameter. Although no significant differences were observed between the case of the static field and the frequency-dependent incident light, the solvent enhanced the first hyperpolarizability by approximately 88%, reaching values around 130×10^{-30} esu, significantly higher than those reported for urea and *p*-nitroaniline, two standard nonlinear optical compounds. The environment emerged as a key factor in the electronic properties of NTAMP. The simple inclusion of the solvent through the PCM induced a significant bathochromic effect (~ 40 nm) in the lowest absorption band $\pi \rightarrow \pi^*$, which was also reflected in the electronic spectra and Stokes shifts.

To conclude this study, a simple analysis of the two-photon absorption cross-section ($\delta_{\text{GM}}^{2\text{PA}}$) was performed, indicating

superior performance compared with standard dyes such as *p*-nitroaniline and even chalcone molecules.

AUTHOR INFORMATION

Corresponding Author

Rodrigo Gester – Instituto de Física, Universidade de São Paulo, São Paulo, São Paulo 05588-090, Brazil; Faculdade de Física, Universidade Federal do Sul e Sudeste do Pará, Marabá, Pará 68507-590, Brazil; orcid.org/0000-0001-6110-424X; Email: gester@unifesspa.edu.br

Authors

Sávio Fonseca – Programa de Pós-Graduação em Química, Universidade Federal do Sul e Sudeste do Pará, Marabá, Pará 68507-590, Brazil; orcid.org/0000-0003-1153-8749

Neidy S. S. dos Santos – Programa de Pós-Graduação em Química, Universidade Federal do Sul e Sudeste do Pará, Marabá, Pará 68507-590, Brazil; orcid.org/0000-0002-0177-8004

Herbert C. Georg – Instituto de Física, Universidade Federal de Goiás, Goiânia, Goiás 74690-900, Brazil

Tertius L. Fonseca – Instituto de Física, Universidade Federal de Goiás, Goiânia, Goiás 74690-900, Brazil; orcid.org/0000-0001-5501-7801

Patricio F. Provasi – Department of Physics, IMIT, Northeastern University, CONICET, Corrientes W 3404 AAS, Argentina

Kaline Coutinho – Instituto de Física, Universidade de São Paulo, São Paulo, São Paulo 05588-090, Brazil; orcid.org/0000-0002-7586-3324

Sylvio Canuto – Instituto de Física, Universidade de São Paulo, São Paulo, São Paulo 05588-090, Brazil; orcid.org/0000-0002-9942-8714

Antônio R. da Cunha – Centro de Ciências de Balsas, Universidade Federal do Maranhão, Balsas, Maranhão 65800-000, Brazil

Complete contact information is available at:
<https://pubs.acs.org/10.1021/acsomega.4c04240>

Funding

The Article Processing Charge for the publication of this research was funded by the Coordination for the Improvement of Higher Education Personnel - CAPES (ROR identifier: 00x0ma614).

Notes

The authors declare no competing financial interest.

ACKNOWLEDGMENTS

This study is financed in part by the Coordenação de Aperfeiçoamento de Pessoal de Nível Superior—Brasil (CAPES), Conselho Nacional de Desenvolvimento Científico e Tecnológico (CNPq), Fundação de Amparo à Pesquisa do Estado de São Paulo (FAPESP), Fundação de Amparo à Pesquisa e ao Desenvolvimento Científico e Tecnológico do Maranhão (FAPEMA), Fundação de Amparo à Pesquisa do Estado de Alagoas (FAPEAL), and Fundação de Amazônica de Amparo a Estudos e Pesquisas (FAPESPA). The authors thank the computational resources provided by (LaMCAD/UFG). P.F.P. would like to acknowledge financial support from Consejo Nacional de Investigaciones Científicas y Técnicas (CONICET), PIP 11220200100467CO and FaCENA-UNNE.

K.C. acknowledges to the National Institute of Science and Technology for Complex Fluids (INCT-FCx), financed by CNPq (141260/2017-3) and FAPESP (2014/50983-3 and 2018/20162-9).

REFERENCES

- (1) Kanis, D. R.; Ratner, M. A.; Marks, T. J. Design and construction of molecular assemblies with large second-order optical nonlinearities. Quantum chemical aspects. *Chem. Rev.* **1994**, *94*, 195–242.
- (2) Delaire, J. A.; Nakatani, K. Linear and Nonlinear Optical Properties of Photochromic Molecules and Materials. *Chem. Rev.* **2000**, *100*, 1817–1846.
- (3) Dalton, L. R.; Sullivan, P. A.; Bale, D. H. Electric field poled organic electro-optic materials: state of the art and future prospects. *Chem. Rev.* **2010**, *110*, 25–55.
- (4) Dok, A. R.; Legat, T.; de Coene, Y.; van der Veen, M. A.; Verbiest, T.; Van Cleuvenbergen, S. Nonlinear optical probes of nucleation and crystal growth: recent progress and future prospects. *J. Mater. Chem. C* **2021**, *9*, 11553–11568.
- (5) Campagnola, P. J.; Loew, L. M. Electric field poled organic electro-optic materials: state of the art and future prospects. *Nat. Biotechnol.* **2003**, *21*, 1356–1360.
- (6) Kim, H. M.; Jeong, B. H.; Hyon, J.-Y.; An, M. J.; Seo, M. S.; Hong, J. H.; Lee, K. J.; Kim, C. H.; Joo, T.; Hong, S. C.; Cho, B. R. Two-photon fluorescent turn-on probe for lipid rafts in live cell and tissue. *J. Am. Chem. Soc.* **2008**, *130*, 4246–4247.
- (7) Reeve, J. E.; Anderson, H. L.; Clays, K. Electric field poled organic electro-optic materials: state of the art and future prospects. *Phys. Chem. Chem. Phys.* **2010**, *12*, 13484–13498.
- (8) Meyers, F.; Marder, S. R.; Pierce, B. M.; Bredas, J. L. Electric Field Modulated Nonlinear Optical Properties of Donor-Acceptor Polyenes: Sum-Over-States Investigation of the Relationship between Molecular Polarizabilities (α , β , and γ) and Bond Length Alternation. *J. Am. Chem. Soc.* **1994**, *116*, 10703–10714.
- (9) Thompson, W. H.; Blanchard-Desce, M.; Hynes, J. T. Two Valence Bond State Model for Molecular Nonlinear Optical Properties. Nonequilibrium Solvation Formulation. *J. Phys. Chem. A* **1998**, *102*, 7712–7722.
- (10) De Oliveira, H. C. B.; Fonseca, T. L.; Castro, M. A.; Amaral, O. A. V.; Cunha, S. Theoretical study of the static first hyperpolarizability of azo-aminone compounds. *J. Chem. Phys.* **2003**, *119*, 8417–8423.
- (11) Murugan, N. A.; Kongsted, J.; Rinkevicius, Z.; Ågren, H. Breakdown of the first hyperpolarizability/bond-length alternation parameter relationship. *Proc. Natl. Acad. Sci. U.S.A.* **2010**, *107*, 16453–16458.
- (12) Castet, F.; Blanchard-Desce, M.; Adamietz, F.; Poronik, Y. M.; Gryko, D. T.; Rodriguez, V. Experimental and Theoretical Investigation of the First-Order Hyperpolarizability of Octupolar Merocyanine Dyes. *ChemPhysChem* **2014**, *15*, 2575–2581.
- (13) Brandão, I.; Franco, L. R.; Fonseca, T. L.; Castro, M. A.; Georg, H. C. Confirming the relationship between first hyperpolarizability and the bond length alternation coordinate for merocyanine dyes. *J. Chem. Phys.* **2017**, *146*, 224505.
- (14) Castet, F.; Gillet, A.; Bures, F.; Plaquet, A.; Rodriguez, V.; Champagne, B. Second-order nonlinear optical properties of Λ -shaped pyrazine derivatives. *Dyes Pigm.* **2021**, *184*, 108850.
- (15) Siqueira, Y.; Lyra, M. L.; Ramos, T. N.; Champagne, B.; Manzoni, V. Unveiling the relationship between structural and polarization effects on the first hyperpolarizability of a merocyanine dye. *J. Chem. Phys.* **2022**, *156*, 014305.
- (16) Fonseca, S.; Modesto-Costa, L.; Milán-Garcés, E.; Andrade-Filho, T.; Gester, R.; da Cunha, A. R. Designing a novel organometallic chalcone with an enormous second-harmonic generation response. *Mater. Today Commun.* **2022**, *31*, 103762.
- (17) Jonin, C.; Dereniowski, M.; Salmon, E.; Gergely, C.; Matczyszyn, K.; Brevet, P.-F. Hyper Rayleigh scattering from DNA nucleotides in aqueous solution. *J. Chem. Phys.* **2023**, *159*, 054303.

- (18) Dehu, C.; Meyers, F.; Hendrickx, E.; Clays, K.; Persoons, A.; Marder, S. R.; Bredas, J. L. Solvent Effects on the Second-Order Nonlinear Optical Response of π -Conjugated Molecules: A Combined Evaluation through Self-Consistent Reaction Field Calculations and Hyper-Rayleigh Scattering Measurements. *J. Am. Chem. Soc.* **1995**, *117*, 10127–10128.
- (19) Kaatz, P.; Shelton, D. P. Polarized hyper-Rayleigh light scattering measurements of nonlinear optical chromophores. *J. Chem. Phys.* **1996**, *105*, 3918–3929.
- (20) Huyskens, F. L.; Huyskens, P. L.; Persoons, A. P. Solvent dependence of the first hyperpolarizability of p-nitroanilines: Differences between nonspecific dipole–dipole interactions and solute–solvent H-bonds. *J. Chem. Phys.* **1998**, *108*, 8161–8171.
- (21) Bourhill, G.; Bredas, J. L.; Cheng, L.-T.; Marder, S. R.; Meyers, F.; Perry, J. W.; Tiemann, B. G. Experimental Demonstration of the Dependence of the First Hyperpolarizability of Donor-Acceptor-Substituted Polyenes on the Ground-State Polarization and Bond Length Alternation. *J. Am. Chem. Soc.* **1994**, *116*, 2619–2620.
- (22) Pauley, M. A.; Wang, C. H.; Jen, A. K. Hyper-Rayleigh scattering studies of first order hyperpolarizability of tricyanovinylthiophene derivatives in solution. *J. Chem. Phys.* **1995**, *102*, 6400–6405.
- (23) Almeida, F. F.; Modesto-Costa, L.; da Cunha, A. R.; Santos, D. A.; Andrade-Filho, T.; Gester, R. Understanding the Stokes shift and nonlinear optical behavior of 1-nitro-2-phenylethane: A sequential Monte Carlo/Quantum Mechanics discussion. *Chem. Phys. Lett.* **2022**, *804*, 139867.
- (24) Tomasi, J.; Mennucci, B.; Cammi, R. Quantum Mechanical Continuum Solvation Models. *Chem. Rev.* **2005**, *105*, 2999–3094.
- (25) Waheeb, A. S.; Kyhoiesh, H. A. K.; Salman, A. W.; Al-Adilee, K. J.; Kadhim, M. M. Metal complexes of a new azo ligand 2-[2'-(5-nitrothiazolyl) azo]-4-methoxyphenol (NTAMP): Synthesis, spectral characterization, and theoretical calculation. *Inorg. Chem. Commun.* **2022**, *138*, 109267.
- (26) Kurtz, H. A.; Dudis, D. S. Quantum Mechanical Methods for Predicting Nonlinear Optical Properties. *Rev. Comput. Chem.* **1998**, *12*, 241–279.
- (27) Zhang, L.; Qi, D.; Zhao, L.; Chen, C.; Bian, Y.; Li, W. Density functional theory study on subtriazaporphyrin derivatives: dipolar/octupolar contribution to the second-order nonlinear optical activity. *J. Phys. Chem. A* **2012**, *116*, 10249–10256.
- (28) Frisch, M. J. et al. *Gaussian 16*, Revision C.01; Gaussian Inc.: Wallingford CT, 2016.
- (29) Lu, T.; Chen, F. Multiwfn: A multifunctional wavefunction analyzer. *J. Comput. Chem.* **2012**, *33*, 580–592.
- (30) Samanta, P. K.; Alam, M. M.; Misra, R.; Pati, S. K. Tuning of hyperpolarizability, and one- and two-photon absorption of donor–acceptor and donor–acceptor–acceptor-type intramolecular charge transfer-based sensors. *Phys. Chem. Chem. Phys.* **2019**, *21*, 17343–17355.
- (31) Aidas, K.; Angeli, C.; Bak, K. L.; Bakken, V.; Bast, R.; Boman, L.; Christiansen, O.; Cimiraglia, R.; Coriani, S.; Dahle, P.; et al. The Dalton quantum chemistry program system. *Wiley Interdiscip. Rev.: Comput. Mol. Sci.* **2014**, *4*, 269–284.
- (32) Parr, R. G.; Yang, W. *Density-Functional Theory of Atoms and Molecules*; Oxford Univ. Press: Oxford, 1989.
- (33) Hohenberg, P.; Kohn, W. Inhomogeneous electron gas. *Phys. Rev.* **1964**, *136*, B864–B871.
- (34) Kohn, W.; Sham, L. J. Self-consistent equations including exchange and correlation effects. *Phys. Rev.* **1965**, *140*, A1133–A1138.
- (35) Chai, J.-D.; Head-Gordon, M. Systematic optimization of long-range corrected hybrid density functionals. *J. Chem. Phys.* **2008**, *128*, 084106.
- (36) Chai, J.-D.; Head-Gordon, M. Long-range corrected hybrid density functionals with damped atom-atom dispersion corrections. *Phys. Chem. Chem. Phys.* **2008**, *10*, 6615–6620.
- (37) Clark, T.; Chandrasekhar, J.; Spitznagel, G. W.; Schleyer, P. V. R. Efficient diffuse function-augmented basis sets for anion calculations. III. The 3-21+G basis set for first-row elements, Li-F. *J. Comput. Chem.* **1983**, *4*, 294–301.
- (38) Krishnan, R.; Binkley, J. S.; Seeger, R.; Pople, J. A. Self-consistent molecular orbital methods. XX. A basis set for correlated wave functions. *J. Chem. Phys.* **1980**, *72*, 650–654.
- (39) Zhao, Y.; Truhlar, D. G. The M06 suite of density functionals for main group thermochemistry, thermochemical kinetics, non-covalent interactions, excited states, and transition elements: two new functionals and systematic testing of four M06-class functionals and 12 other functionals. *Theor. Chem. Acc.* **2008**, *120*, 215–241.
- (40) Yanai, T.; Tew, D.; Handy, N. A new hybrid exchange-correlation functional using the Coulomb-attenuating method (CAM-B3LYP). *Chem. Phys. Lett.* **2004**, *393*, 51–57.
- (41) Miertuš, S.; Scrocco, E.; Tomasi, J. Electrostatic interaction of a solute with a continuum. A direct utilization of AB initio molecular potentials for the prevision of solvent effects. *Chem. Phys.* **1981**, *55*, 117–129.
- (42) Miertuš, S.; Tomasi, J. Approximate Evaluations of the Electrostatic Free Energy and Internal Energy Changes in Solution Processes. *Chem. Phys.* **1982**, *65*, 239–245.
- (43) Shalin, N. I.; Fominykh, O. D.; Balakina, M. Y. Effect of acceptor moieties on static and dynamic first hyperpolarizability of azobenzene chromophores. *Chem. Phys. Lett.* **2019**, *717*, 21–28.
- (44) Rtibi, E.; Champagne, B. Density Functional Theory Study of Substitution Effects on the Second-Order Nonlinear Optical Properties of Lindquist-Type Organo-Imido Polyoxometalates. *B. Symmetry* **2021**, *13*, 1636.
- (45) Reichardt, C. Solvatochromic dyes as solvent polarity indicators. *Chem. Rev.* **1994**, *94*, 2319–2358.
- (46) Marder, S. R.; Gorman, C. B.; Meyers, F.; Perry, J. W.; Bourhill, G.; Brédas, J. L.; Pierce, B. M. A unified description of linear and nonlinear polarization in organic polymethine dyes. *Science* **1994**, *265*, 632–635.
- (47) Franco, L. R.; Brandão, I.; Fonseca, T. L.; Georg, H. C. Elucidating the structure of merocyanine dyes with the ASEC-FEG method. Phenol blue in solution. *J. Chem. Phys.* **2016**, *145*, 194301.
- (48) Shalin, N. I.; Phrolycheva, Y. A.; Fominykh, O. D.; Balakina, M. Y. Solvent effect on static and dynamic first hyperpolarizability of azochromophore with tricyanopyrrole acceptor moiety. *J. Mol. Liq.* **2021**, *330*, 115665.
- (49) Alam, M. M.; Kundi, V.; Thankachan, P. P. Solvent effects on static polarizability, static first hyperpolarizability and one- and two-photon absorption properties of functionalized triply twisted Möbius annulenes: a DFT study. *Phys. Chem. Chem. Phys.* **2016**, *18*, 21833–21842.
- (50) Quertinmont, J.; Champagne, B.; Castet, F.; Hidalgo Cardenuto, M. Explicit versus Implicit Solvation Effects on the First Hyperpolarizability of an Organic Biphotochrome. *J. Phys. Chem. A* **2015**, *119*, 5496–5503.
- (51) Ferrighi, L.; Frediani, L.; Cappelli, C.; Salek, P.; Ågren, H.; Helgaker, T.; Ruud, K. Density-functional-theory study of the electric-field-induced second harmonic generation (EFISHG) of push–pull phenylpolyenes in solution. *Chem. Phys. Lett.* **2006**, *425*, 267–272.
- (52) Bartkowiak, W.; Lipiński, J. Conformation and solvent dependence of the first molecular hyperpolarizability of piridinium-N-phenolate betaine dyes. Quantum chemical calculations. *J. Phys. Chem. A* **1998**, *102*, 5236–5240.
- (53) Marrazzini, G.; Giovannini, T.; Egidi, F.; Cappelli, C. Calculation of Linear and Non-linear Electric Response Properties of Systems in Aqueous Solution: A Polarizable Quantum/Classical Approach with Quantum Repulsion Effects. *J. Chem. Theory Comput.* **2020**, *16*, 6993–7004.
- (54) Gester, R.; Siqueira, M.; Cunha, A. R.; Araújo, R. S.; Provasi, P. F.; Canuto, S. Assessing the dipolar–octupolar NLO behavior of substituted thiosemicarbazone assemblies. *Chem. Phys. Lett.* **2023**, *831*, 140807.
- (55) Damasceno, M. V. A.; Cunha, A. R.; Provasi, P. F.; Pagola, G. I.; Siqueira, M.; Manzoni, V.; Gester, R.; Canuto, S. Modulation of the NLO properties of p-coumaric acid by the solvent effects and proton dissociation. *J. Mol. Liq.* **2024**, *394*, 123587.

(56) Beerepoot, M. T. P.; Friese, D. H.; List, N. H.; Kongsted, J.; Ruud, K. Benchmarking two-photon absorption cross sections: performance of CC2 and CAM-B3LYP. *Phys. Chem. Chem. Phys.* **2015**, *17*, 19306–19314.

(57) Wielgus, M.; Michalska, J.; Samoc, M.; Bartkowiak, W. Two-photon solvatochromism III: Experimental study of the solvent effects on two-photon absorption spectrum of p-nitroaniline. *Dyes Pigments* **2015**, *113*, 426–434.

(58) Ramos, T. N.; Silva, D. L.; Cabral, B. J. C.; Canuto, S. On the spectral line width broadening for simulation of the two-photon absorption cross-section of para-nitroaniline in liquid environment. *J. Mol. Liq.* **2020**, *301*, 112405.

(59) Abegão, L. M.; Fonseca, R. D.; Santos, F. A.; Souza, G. B.; Barreiros, A. L. B. S.; Barreiros, M. L.; Alencar, M. A. R. C.; Mendonça, C. R.; Silva, D. L.; De Boni, L.; Rodrigues, J. J., Jr. Second- and third-order nonlinear optical properties of unsubstituted and mono-substituted chalcones. *Chem. Phys. Lett.* **2016**, *648*, 91–96.

(60) Araújo, R. S.; Sciuti, L. F.; Cocca, L. H. Z.; Lopes, T. O.; Silva, A. A.; Abegão, L. M.; Valle, M. S.; Rodrigues, J. J., Jr.; Mendonça, C. R.; De Boni, L.; Alencar, M. A. R. C. Comparing two-photon absorption of chalcone, dibenzylideneacetone and thiosemicarbazone derivatives. *Opt. Mater.* **2023**, *137*, 113510.